Civil and Environmental Engineering
Vol. 0, Issue 0, DOI: 10.2478/cee-2026-0077

Mechanical Behaviour and Evolution of Rock Loosening Zone in in-situ Reconstruction and Expansion Construction of Highway Tunnels

Weisheng SU[1], Zhi LIN[2,*], Hongyun YANG[2], Siyu DANG[1], Han WU[2]

[1] Guangxi Xinfazhan Communication Group Co., Ltd. Guangxi, China

[2] State Key Laboratory of Bridge and Tunnel Engineering, Chongqing Jiaotong University, Chongqing, China

* corresponding author: zhilin@cqjtu.edu.cn

Date of Submission: 04 November 2025
Revision Date: 18 December 2025
Date of Acceptance: 21 December 2025

Civil and Environmental Engineering
Journal of the Faculty of Civil Engineering | University of Žilina

Abstract

This study systematically investigated the construction mechanical behaviour and surrounding rock loose zone evolution patterns during the in-situ reconstruction and expansion of highway tunnels, utilizing the GDEM discrete element program integrated with field monitoring data to analyse the excavation process of the reference Tingxin Tunnel project. The key conclusions are as follows: During the in-situ expansion of the bidirectional four-lane separated tunnel, the vertical stresses at various monitoring points primarily exhibit tensile stresses with a gradual decreasing trend; the thickness of the surrounding rock loose zone increased by 76.62% before and after the expansion construction, with the entire inter-tunnel rock wall entering the loose zone post-expansion, and the maximum extension occurring at the shoulder positions. Therefore, implementing pre-support or reinforcement measures for the surrounding rock prior to in-situ excavation in close-spaced tunnels can significantly enhance the tensile strength of the rock mass above the tunnel crown and improve the load-bearing capacity of the inter-tunnel rock wall. This holds substantial engineering significance for improving construction safety, mitigating collapse risks and associated economic losses, and accelerating project progress.

Keywords

Highway tunnel; In-situ expansion; Construction mechanical behaviour; Surrounding rock loose zone.

1. Introduction

Since 2000, the total mileage of highway tunnels in China has been increasing at an average rate of 1152.3 kilometres per year (Yang H. et al. 2025). The number and total mileage of highway tunnels in China from 2000 to 2024 are shown in Figure 1. Although the number and total mileage of tunnels have been increasing, the traffic volume has also been growing exponentially. Many tunnels built in earlier years were designed as two-lane tunnels, which can no longer meet the rapidly growing traffic demand. Furthermore, during their long-term operation, the tunnel support structures have been subjected to varying degrees of damage for various reasons, making it impossible for these tunnels to meet the normal usage requirements. It should be noted that similar problems related to insufficient tunnel capacity and aging support structures are not limited to China (Krupík, P. 2025). With the rapid development of transportation networks worldwide, in-situ tunnel renovation and expansion have also become important engineering solutions in many countries. Therefore, research on tunnel expansion has attracted increasing attention in both domestic and international tunnel engineering fields.

Both domestic and international research generally agree that tunnel enlargement often leads to asymmetric deformation, stress concentration, and expansion of plastic zones in the surrounding rock. Zheng, X et al. (2025) suggested that the impact of excavation on the original or already expanded tunnels is minimal, and that during excavation, the tensile stresses in the surrounding rock mainly occur at the crown, shoulder, and waist of the arch. Zhang S. (2019) found through numerical simulations that regardless of the excavation method used, the maximum horizontal stress in the surrounding rock is located at the tunnel's arch foot. When the in-situ expansion method is adopted, surface settlement, crown settlement, and tunnel convergence are significantly greater than those in small clearance expansion. Hernández Y. et al (2019) revealed a direct correlation with the increase of cover-to-tunnel diameter ratio and support pressure values during excavation. Zhang J. et al. (2021) conducted numerical simulations and found that the maximum bending moment occurs at the arch shoulder when using the step-by-step method for tunnel expansion.

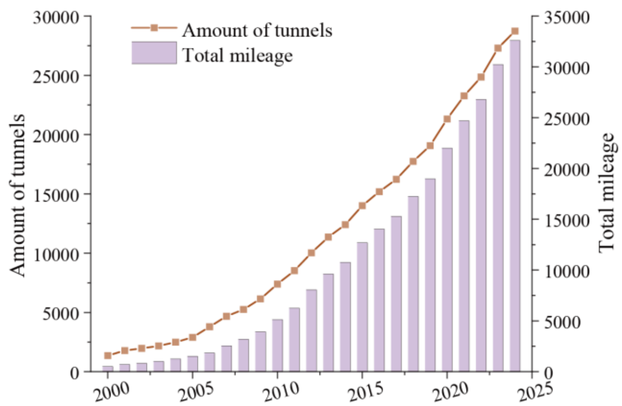

Figure 1: Number and total mileage of highway tunnels in China from 2000 to 2024 (Ministry of Transport of the People's Republic of China. 2025)

Luo, Y. et al. (2020) promoted that when a large span tunnel is excavated, the rock mass is disturbed and difficult to form a load-bearing arch under shallow depth region, which will result in the complicated structural deformation. Shu Y. et al. (2012) found that in the expansion of tunnels with small clearances, the yield zone in the surrounding rock is primarily concentrated at the arch foot, with the axial force in the outer anchors being approximately 4 to 5 times greater than that in the inner anchors. Hu J. et al. (2011) suggested that during tunnel expansion, the deformations of the surrounding rock at the crown and arch shoulder are the greatest and exhibit asymmetry, with surrounding rock stresses also showing asymmetrical behaviour. Feng G. et al. (2017) observed that after tunnel expansion, surface settlement slightly shifts toward the side away from the existing tunnel, presenting asymmetry. Wan M. et al. (2006) found that in large-span tunnels, the settlement at the crown is greater than the horizontal convergence, and horizontal displacements of the support structure mainly occur at the arch waist during expansion. Hu, J et al. (2011) noted that during in-situ tunnel expansion, the radius of the plastic zone in the surrounding rock is influenced by excavation methods, stress redistribution, and spatial effects, and changes over time. Zhong Y. (2019) observed that during the benching tunnelling method, the loosened zone in the surrounding rock is located at a depth of 6 to 9 meters at the crown, 0 to 6 meters at the side walls, and the plastic zone in the surrounding rock is about 3 meters.

In addition, research on the theoretical understanding of the surrounding rock loosened zone in highway tunnels has made considerable progress, resulting in the development of seven representative loosening zone hypotheses, including the natural balance arch theory, elastic medium theory, and plastic medium theory (Meng Q. et al.2025, Wu Z. et al. 2009, Yan S. et al. 2024). These theories have been widely recognized and applied as fundamental analytical frameworks for evaluating surrounding rock stability in tunnel engineering, providing important theoretical support for both new tunnel construction and tunnel expansion projects.

Although valuable conclusions have been obtained from previous studies, systematic investigations on the evolution characteristics of loosened zones during in-situ tunnel expansion are still insufficient. Therefore, this paper aims to explore the evolution of surrounding rock loosened zones in in-situ tunnel expansion, enriching the research on the mechanical behaviour of tunnel expansion and providing theoretical guidance for similar tunnel expansion projects.

2. Engineering Background

This study is based on the in-situ expansion project of the Tingxin Tunnel on the Hezhou to Bama Expressway (Du'an to Bama section) in Guangxi. The original Tingxin Tunnel is a bidirectional, four-lane separated tunnel located in an area with poor geological conditions, where the surrounding rock primarily consists of class IV and class V (Ministry of Transport of the People's Republic of China. 2018). Additionally, the tunnel is shallowly buried, posing significant safety and construction schedule risks. The original tunnel cannot accommodate the increased traffic volume, necessitating its expansion to a bidirectional six-lane separated tunnel. After expansion, the clear width (H) is 19.23 meters, the clear height (B) is 12.94 meters, and the clear span is 14.61 meters, with a flatness ratio (H/B) of 0.67. The expanded tunnel is classified as a large-span tunnel, and the expansion method is designed as a one-sided excavation with a benching tunnelling method. In areas with Class V surrounding rock, both vertical temporary supports and temporary horizontal supports will be installed during construction, while in areas with Class IV surrounding rock, only vertical temporary supports will be used.

In the expansion project of the Tingxin Tunnel, boreholes were arranged at intervals of 2 meters between the stake numbers ZK435+368 to ZK435+374 and YK435+326 to YK435+332, with a total of eight boreholes. These boreholes were positioned at the arch waist of the excavation side. The rock cores obtained from these boreholes were subjected to six sets of laboratory tests, including uni-axial compression tests, direct shear tests, and longitudinal wave velocity tests, to analyse the mechanical properties of the surrounding rock in the test section as shown in Figure 2. The mechanical properties of the surrounding rock were shown in Table 1.

Figure 2: Rock samples obtained in Tingxin tunnel

The mechanical properties of surrounding rock are shown in Table 1 and Table 2.

Table 1: Rock experiment report of Tingxin tunnel

	Density(g/cm^3)	Elastic modulus (GPa)	Poisson's ratio	Uni-axial compressive strength (MPa)	Cohesive (MPa)	Friction angle (°)	P-wave velocity(m/s)
ZK435+368	2.51	1.43	0.33	24.30	0.60	40.76	3160
ZK435+370	2.47	1.47	0.34	26.87	0.73	42.40	2930
ZK435+372	2.50	1.50	0.31	29.10	0.79	40.51	3184
ZK435+374	2.52	1.40	0.35	28.05	0.63	41.12	3086
YK435+326	2.19	0.87	0.41	13.52	0.24	28.53	2204
YK435+328	2.10	0.93	0.40	15.20	0.29	29.13	2192
YK435+330	2.12	0.91	0.42	14.95	0.23	30.47	2084
YK435+332	2.13	0.86	0.44	14.38	0.19	29.57	2050

Table 2: Mechanical property of surrounding rock

Surrounding rock grade	Unit weight γ (kN/m^3)	Elastic modulus E (GPa)	Poisson's ratio μ	Cohesive C (MPa)	Tensile strength f_{ck} (MPa)	Friction angle φ (°)	Dilation angle (°)
III	25	10	0.25	1	4	44	15
IV	23	3	0.3	0.5	1	35	10
V V̄	20	1.5	0.35	0.2	0.5	30	7

The comparison of the in-situ rock test results with the recommended values of the surrounding rock's mechanical parameters in the code (Li L. et al. 2020) shows that the test section's surrounding rock has a higher density, cohesion, and internal friction angle, which are close to the recommended values for Class III surrounding rock in the code. However, during excavation, the exposed tunnel mainly consists of highly weathered sandstone and moderately weathered sandstone, as shown in Figure 3. These rock masses have a relatively well-developed system of joint fractures, which leads to poor overall mechanical properties and geotechnical stability of the surrounding rock mass. As a result, incidents such as loosening and instability of the surrounding rock are prone to occur during excavation. Therefore, in the preliminary geophysical investigation stage or during tunnel expansion construction, the surrounding rock is often classified as Class IV or Class V.

Figure 3: Revealed rock mass during expansion of Tingxin tunnel

3. Validation of GDEM

This paper simulates the uni-axial compression and Brazilian splitting tests of Class IV surrounding rock to compare the results with in-situ laboratory experiments conducted by other researchers, thereby validating the feasibility and accuracy of the GDEM. The parameters for the surrounding rock are all taken from Table 2 to Table 4.

3.1. Uni-axial Compression

In GDEM, the uni-axial compression of Class IV surrounding rock was modelled using a prismatic specimen measuring 10×20 cm, discretized with a uniform element size of 2 mm. The Mohr–Coulomb constitutive model was adopted, and a quasi-static downward velocity boundary of 1×10^{-6} mm/s was applied at top surface in Y-direction.

The simulation indicates shear-dominated failure under uni-axial loading. A primary shear band developed with an inclination of approximately 42° to the loading axis. The peak shear plastic strain on the failure plane reached 0.02395, with pronounced concentrations near the two tips of the plane. Along the failure plane, the apparent thickness of the zone where the combined damage factor attains 1 is about 11.4–12.7 mm. Contour maps of shear plastic strain and combined damage factor are shown in Figure 4.

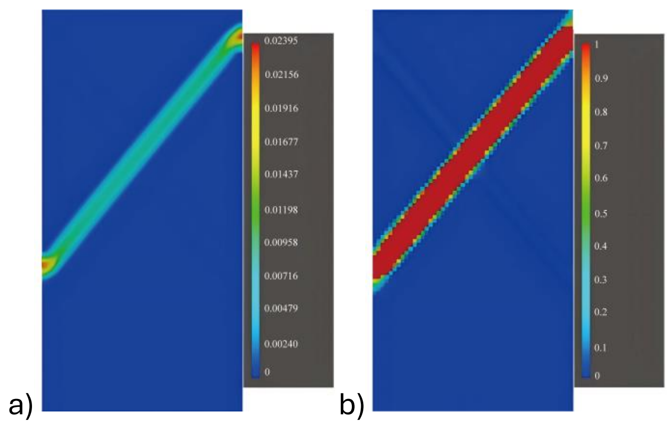

Figure 4: a) Shear strain map; b) Combined damage factor cloud map

During uni-axial compression loading, the specimen progressed through three characteristic stages: the elastic stage, the plastic stage, and the failure stage. In the elastic stage, the peak stress of the specimen reached 10.08 MPa, corresponding to a peak strain of 315με. Based on monitoring data from the fracture plane, the vertical stress-vertical strain relationship was plotted in Figure 5.

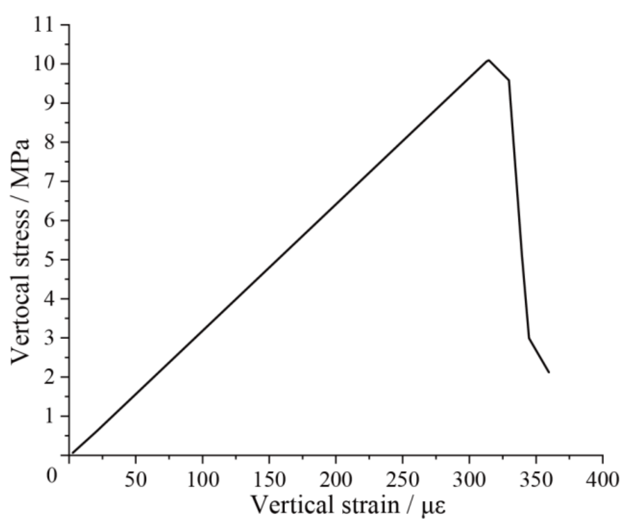

Figure 5: Vertical stress-strain curve

3.2. Brazilian Splitting Test

This study utilized the GDEM to simulate the Brazilian splitting test on Class IV surrounding rock, with a specimen radius of 20 mm and an element size of 1 mm. The constitutive model for elements was a linear elastic model, while the contact surfaces employed a fracture energy model. A quasi-static downward load was applied at the top in Y-direction at a velocity of 1×10^{-6} mm/s.

The X-direction displacements and the tensile damage factor cloud map are shown in Figure 6.

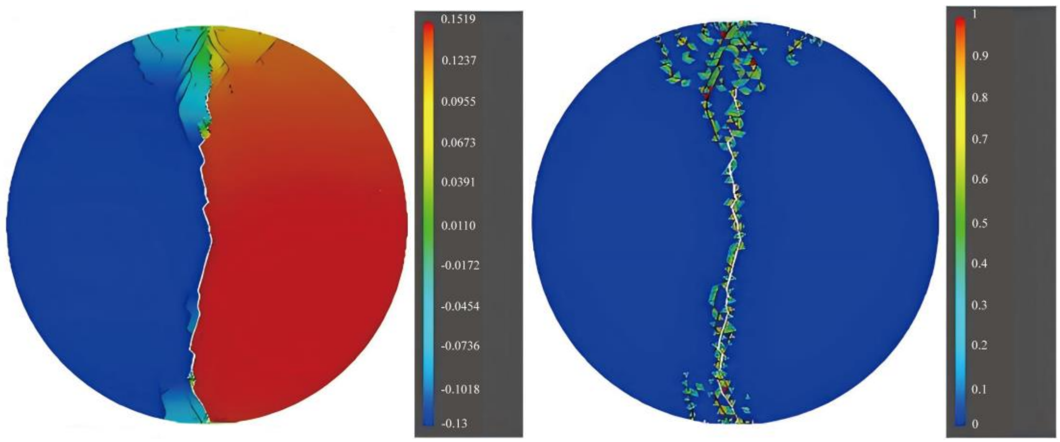

Figure 6: a) Displacement at x-direction; b) Tensile damage factor map

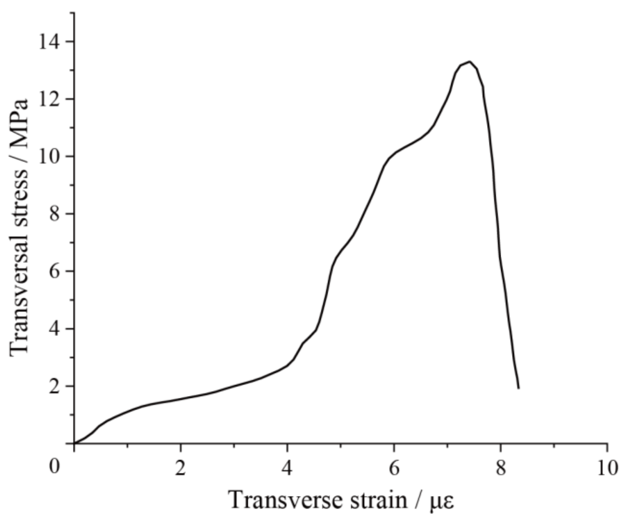

Figure 7: Relationship between transverse stress and strain

During the tensile loading process, the specimen progressed through three stages: the elastic stage, the plastic stage, and the failure stage. The tensile strength of the specimen was 13.2931 MPa, corresponding to a peak strain of 7.33119×10^{-6}. The relationship between the lateral stress and lateral strain is shown in Figure 7.

A comparative analysis of the surrounding rock's uni-axial compression and Brazilian splitting test results simulated using the GDEM software with experimental results from other researchers (You M. et al.2011, Lin k. et al. 2013, Yang S. et al. 2015, Wu Y. et al.2024, Chen L. et al. 2020, Huang Z. et al. 2021) indicates that the software effectively replicates the deformation characteristics, failure processes, and outcomes of the surrounding rock. This demonstrates a high degree of agreement with actual experiments and the reference engineering project, thereby fulfilling the requirements for the reliability and accuracy of the numerical simulation software in this study.

4. Numerical Simulation

4.1. Model Settings

In the reference engineering project, the clear width of the three-lane tunnel after the expansion of the Tingxin Tunnel is designed as 19.23 m, while the minimum clear spacing between the two tunnel portals is 117 m, which is significantly greater than five times the clear width (5×19.23 m ≈96.15 m). Consequently, the expansion process of the Tingxin Tunnel has negligible effects on the stress and deformation responses of the adjacent tunnel. Therefore, for numerical simulation of the in-situ tunnel expansion, a single-tunnel model can be established.

GDEM was employed to conduct numerical simulations of the in-situ expansion construction of the Tingxin Tunnel at the cross-section ZK435+150. The simulations consider varying surrounding rock classification and excavation widths. Models were established for newly constructed two-lane, three-lane, and four-lane tunnels, as well as the "two-to-three" (expansion from two-lane to three-lane) and "two-to-four" (expansion from two-lane to four-lane) scenarios. In subsequent sections, these five distinct excavation conditions are denoted as A, B, C, D, and E, respectively. The analyses were performed under Class III, Class IV, and Class V surrounding rock conditions, resulting in a total of 15 combined scenarios, as detailed in Table 3.

Table 3: Numerical simulation conditions

Combination of conditions	A (Newly constructed two-lane tunnel model)	B (Newly constructed three-lane tunnel model)	C (Newly constructed four-lane tunnel model)	D (Expansion from two-lane to three-lane)	E (Expansion from two-lane to four-lane)
Class III surrounding rock	A+III	B+III	C+III	D+III	E+III
Class IV surrounding rock	A+IV	B+IV	C+IV	D+IV	E+IV
Class V surrounding rock	A+V	B+V	C+V	D+V	E+V

The model width is 200 m, with a maximum height of 180 m at the top, and the upper boundary is modelled based on the actual ground surface. The left and right boundaries of the tunnel model are positioned more than five times the rough tunnel span away from the tunnel rough walls, and the bottom boundary is similarly distanced from the tunnel invert by more than five times the span, to minimize boundary effects. The constitutive model for the support structure employs a linear elastic model, while the surrounding rock elements use the Mohr-Coulomb model, and the contact interfaces adopt the Mohr-Coulomb brittle fracture model. The maximum element size is 3 m, primarily located outside the tunnel excavation model, whereas the minimum element size is 0.1 m, concentrated at the tunnel support structure and the interfaces between the surrounding rock and the support. The model schematic is illustrated in Figure 8.

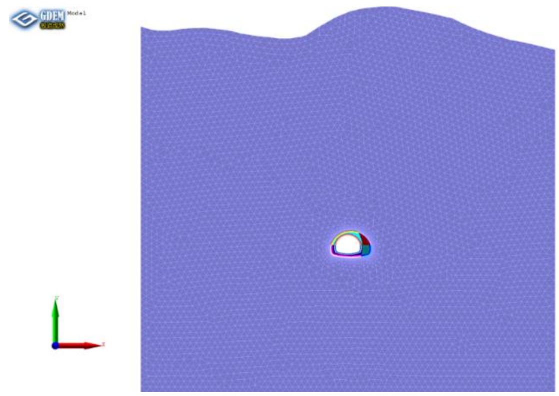

Figure 8: GDEM numerical model for in-situ tunnel expansion

The simulation adopts the one-sided excavation scheme and the post-expansion support scheme. The design parameters for the tunnel support structures are detailed in Table 4.

Table 4: Parameters for tunnel linings

	Surrounding rock classification	Primary support		Secondary lining	
		Concrete grade	Thickness / cm	Concrete grade	Thickness / cm
Two-lane tunnel model	III	C25	10	C30	35
	IV	C25	23	C35	40
	V	C25	24	C35	45
Three-lane tunnel model	III	C25	12	C35	40
	IV	C25	24	C35	45
	V	C25	26	C35	55
Four-lane tunnel model	III	C25	14	C35	45
	IV	C25	26	C35	50
	VV	C25	28	C35	60

The mechanical parameters of the surrounding rock used in this numerical simulation were comprehensively determined based on field measurements from the reference engineering project and relevant code specifications, as detailed in Table 2.

Due to the absence of in-situ tests for the surrounding rock joints, the joint parameters were established in this study according to the Generalized Hoek-Brown strength criterion, with reference to experiences from other underground projects.

The Generalized Hoek-Brown strength criterion is expressed by **Equation (1):**

$$\sigma_1=\sigma_3+\sigma_{ci}\left(m_b\frac{\sigma_3}{\sigma_{ci}}+s\right)^{\alpha} \tag{1}$$

Where:

σ_1 - *definition of the maximum principal stress at rock mass failure*,

σ_3 - *definition of minimum principal stress at failure*,

σ_{ci} - *definition of the uni-axial compressive strength of the intact rock blocks constituting the rock mass*,

m_b - *the Hoek-Brown constant for the rock mass, given by **Equation (2):***

$$m_b=m_i exp\left(\frac{GSI-100}{28-14D}\right) \tag{2}$$

Where:

m_i - *definition of the Hoek-Brown constant for the intact rock blocks*,

GSI - definition of the Geological Strength Index,

D - the disturbance factor accounting for the degree of disturbance to the rock mass due to blasting or stress relaxation.

The rock mass material parameters *s* and *α* are given by **Equation (3)** and **Equation (4)**, respectively:

$$s=exp\left(\frac{GSI-100}{9-3D}\right) \tag{3}$$

$$\alpha=\frac{1}{2}+\frac{1}{6}\left(e^{-\frac{GSI}{15}}-e^{\frac{20}{3}}\right) \tag{4}$$

The uni-axial compressive strength of the rock mass, σ_c, is given by **Equation (5)**:

$$\sigma_c=\sigma_{ci}s^{\alpha} \tag{5}$$

The tensile strength of the rock mass, σ_c, is given by **Equation (6)**:

$$\sigma_t=-\frac{S\sigma_{ci}}{m_b} \tag{6}$$

When the uni-axial compressive strength of the intact rock blocks constituting the rock mass is less than 100 MPa, refer to **Equation (7)**:

$$E_m=\left(1-\frac{D}{2}\right)\sqrt{\frac{\sigma_{ci}}{100}}*10^{\left(\frac{GSI-10}{40}\right)} \tag{7}$$

When the uni-axial compressive strength of the intact rock blocks constituting the rock mass exceeds 100 MPa, refer to **Equation (8)**:

$$E_m=\left(1-\frac{D}{2}\right)*10^{\left(\frac{GSI-10}{40}\right)} \tag{8}$$

$$\phi^{'}=sin^{-1}\left[\frac{6\alpha m_b(s+m_b\sigma_{3n}^{'})^{\alpha-1}}{2(1+\alpha)(2+\alpha)+6\alpha m_b(s+m_b\sigma_{3n}^{'})^{\alpha-1}}\right] \tag{9}$$

$$c^{'}=\frac{\sigma_c\left[(1+2\alpha)s+(1-\alpha)m_b\sigma_{3n}^{'}\left(s+m_b\sigma_{3n}^{'}\right)^{\alpha-1}\right.}{(1+\alpha)(2+\alpha)\sqrt{1+\frac{6\alpha m_b\left(s+m_b\sigma_{3n}^{'}\right)^{\alpha-1}}{(1+\alpha)(2+\alpha)}}} \tag{10}$$

$$\sigma_{3n}=\frac{\sigma_{3max}^{'}}{\sigma_{ci}} \tag{11}$$

Where:

$\sigma_{3max}^{'}$ - definition of *the upper limit of the minimum principal stress under the relationship between the Hoek-Brown criterion and the Mohr-Coulomb criterion*, *given by **Equation (12)***:

$$\sigma'_{3max}=0.72(\sigma'_{cm}/\rho gH)^{-0.91} \tag{12}$$

Where*:*

ρ - *definition of the rock mass density,*

g - *definition of the gravitational acceleration,*

H - *definition of the slope height,*

σ'_{cm} - *definition of the overall rock mass strength. When* $\sigma_t<\sigma'_3<0.25\sigma_{ci}$, *it is given by* ***Equation (13)***:

$$\sigma'_{cm}=\frac{\sigma_{ci}[m_b+4s-\alpha(m_b-8s)](s+m_b/4)^{\alpha-1}}{2(1+\alpha)(2+\alpha)} \tag{13}$$

In the discontinuous mechanics analysis, the structural planes of interest extend beyond the peak strengths of major faults and shear zones to encompass the geometric and mechanical characteristics of other structural planes as well. The geometric features include the statistical distribution characteristics of structural planes - particularly random joints - such as their orientation, spacing, and length. The mechanical features, on the other hand, involve the deformation performance (e.g., stiffness) and strength properties of these structural planes. Due to the absence of in-situ tests for the structural planes in this study, the parameters were primarily determined using empirical formulas, with reference to experiences from other underground projects.

$$k_n=\frac{E_mE_r}{s(E_r-E_m)} \tag{14}$$

$$k_s=\frac{G_mG_r}{s(G_r-G_m)} \tag{15}$$

Where*:*

k_n - *definition of the normal stiffness,*

k_s - *definition of the shear stiffness,*

E_m - *definition of the deformation modulus of the rock mass,*

E_r - *definition of the deformation modulus of the intact rock,*

G_m - *definition of the shear modulus of the rock mass,*

G_r - *the shear modulus of the intact rock*.

Based on laboratory tests of rock cores obtained from drilling in the Tingxin Tunnel and preliminary geo-technical survey data, combined with calculations from Equations (1) to (15), the mechanical parameters properties of joint were determined, as presented in Table 5 and Table 6.

Table 5: Mechanical property of jointing the surrounding rock

Surrounding rock classification	**Normal Stiffness.** k_n **(GPa/m)**	**Shear stiffness** k_s **(GPa/m)**	**Tensile strength** σ_t **(MPa)**	**Cohesion (MPa)**	**Friction angle** φ **(°)**
III	200	200	1	0.5	44
IV	60	60	0.25	0.25	35
VV	30	30	0.13	0.05	22

Table 6: Mechanical parameters of tunnel lining

Material	Unit weight γ (kN/m³)	Elastic modulus E (GPa)	Poisson's ratio μ	Tensile strength f_{ck} (MPa)
C25 Shooting concrete	22	26	0.2	1.27
C30 Reinforced concrete	25	30	0.2	2.2
C35 Reinforced concrete	25	31.5	0.2	2.5
Rebar	78.5	200	0.2	1000

4.2. Excavation Steps

The in-situ tunnel expansion was simulated using the benching method, following the construction sequence in Table 7.

Table 7: Construction sequence of in-situ tunnel expansion using benching method

Sequence	Construction
1	Removal of the original lining and excavation of the upper bench.
2	Removal of the original lining and excavation of the lower bench, with installation of temporary support.
3	Excavation of the upper pilot heading in the side drift, followed by placement of a temporary invert for the upper side bench.
4	Excavation of the lower pilot heading in the side drift, and removal of the temporary support and temporary invert; Implementation of the primary support, followed by full-face casting of the secondary lining concrete in a single pour.

The construction sequence is illustrated in Figure 9.

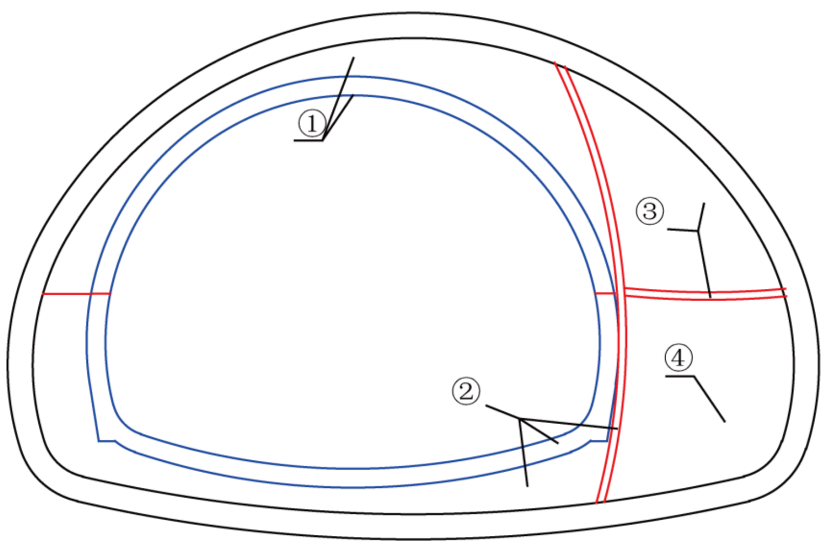

Figure 9: Expansion sequence of the numerical simulation for the Tingxin tunnel

4.3. Monitoring Schedule

This study focuses solely on the stress and deformation of the post-expansion support structures, as well as the displacement and stress of the surrounding rock. Since the original tunnel lining is removed at the initial stage, no monitoring is conducted on the original lining. For the post-expansion lining, monitoring points are established to track crown settlement, shoulder convergence, and waist convergence. Additionally, three rings of monitoring points - totalling 20 points - are arranged at the locations of expanded lining, 0.5 d, 1 d, and 2 d from the tunnel (where d is the equivalent diameter). The locations of the monitoring points in the numerical simulation align with those in the model tests. Data from the monitoring points are collected every 100 computational steps. The monitoring point layout scheme is illustrated in Figure 10.

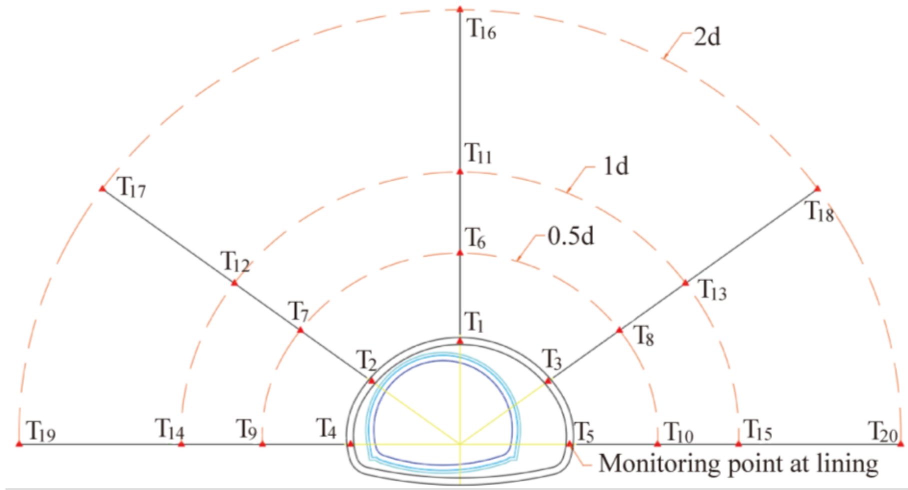

Figure 10: Layout of monitoring points

5. Results

5.1. Mechanical Behaviour During Construction

The stress distributions at the monitoring points for newly constructed and expanded tunnels under multiple scenarios are illustrated from Figure 11 to Figure 14. Letters from A to E correspond to the 5 excavation conditions listed in Table 3.

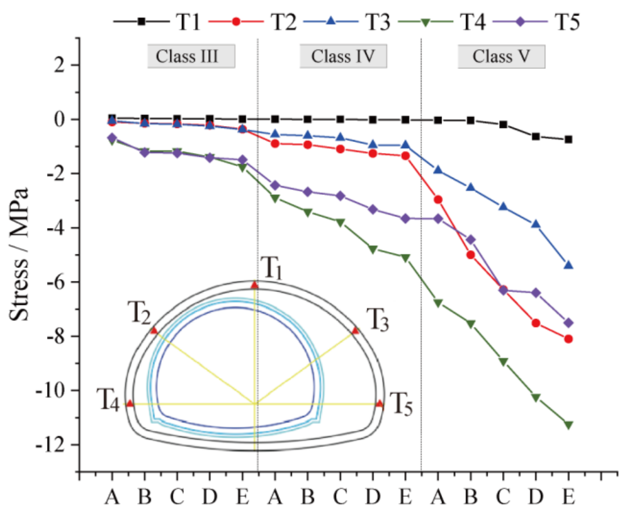

Figure 11: Stress variation curves at monitoring points of the lining

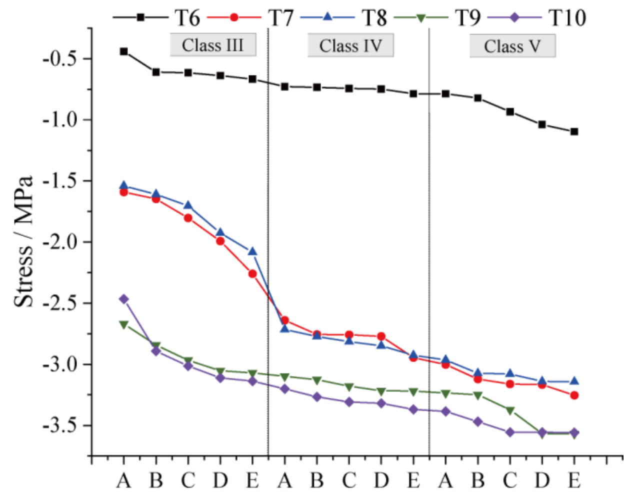

Figure 12: Stress variation curves at monitoring points at the 0.5 d location

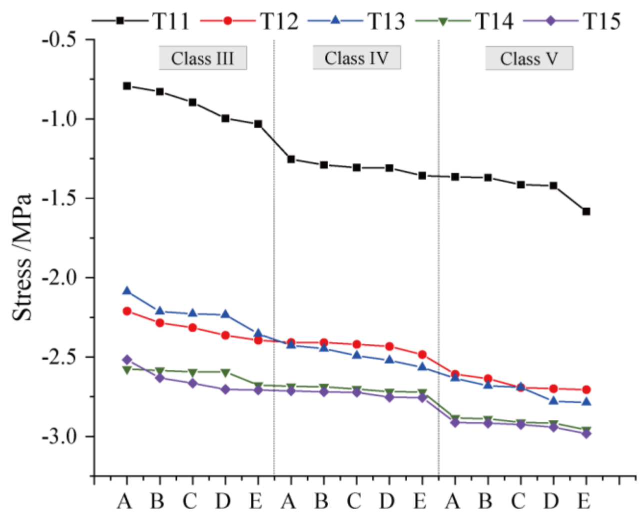

Figure 13: Stress variation curves at monitoring points at the 1 d location

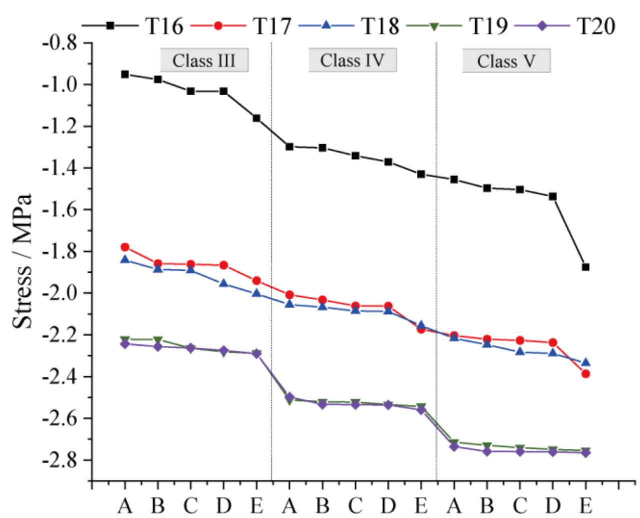

Figure 14: Stress variation curves at monitoring points at the 2 d location

Results indicate that:

Among the monitoring points in different locations, the surrounding rock stresses follow a consistent order: crown < waist < invert. Under the same surrounding rock classification, the surrounding rock stresses at each monitoring point increase progressively with increasing excavation width; under the same excavation width, the stresses increase progressively with decreasing surrounding rock grade, meaning that deteriorating construction conditions lead to greater surrounding rock stresses.

Under identical excavation widths, the surrounding rock stresses in newly constructed three-lane or four-lane tunnels are lower than those in in-situ expanded tunnels. Therefore, in in-situ tunnel expansion projects, the loads calculated using the surrounding rock load method for new tunnels (Dayong H. et al. 2025) are conservatively low compared to actual loads, necessitating adjustments to enhance design safety.

5.2. Displacement

The simulation results for the vertical displacement distributions at monitoring points under multiple scenarios are presented in Figure 15 to Figure 18. Letters from A to E correspond to the 5 excavation conditions listed in Table 3.

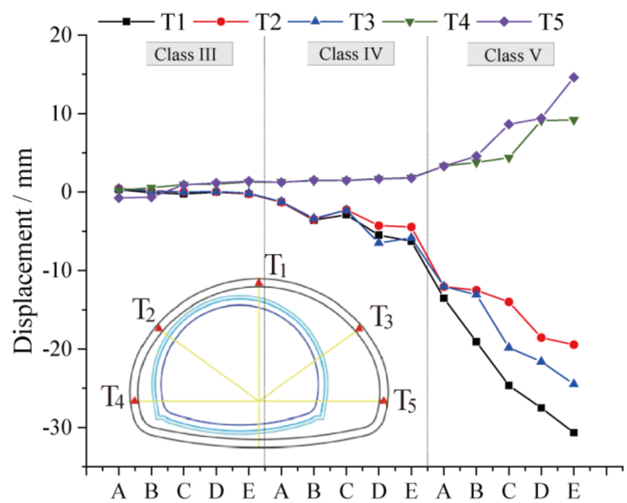

Figure 15: Displacement curves at monitoring points of the lining

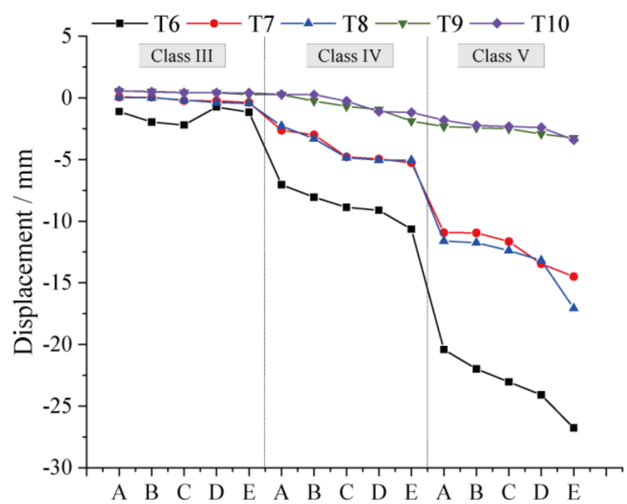

Figure 16: Displacement curves at monitoring points at the 0.5 d location

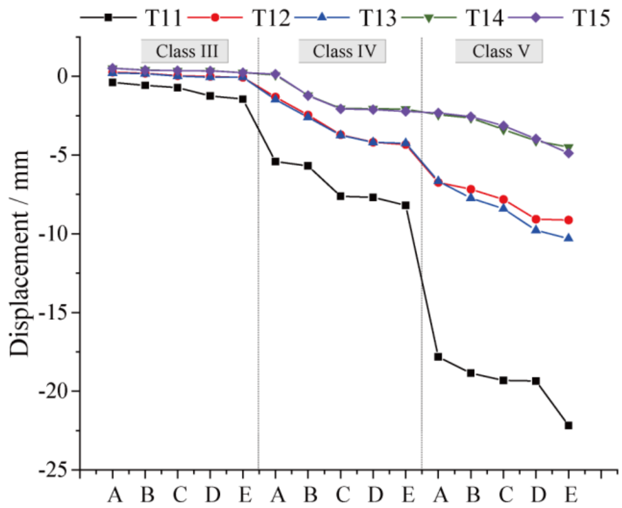

Figure 17: Displacement curves at monitoring points at the 1 d location

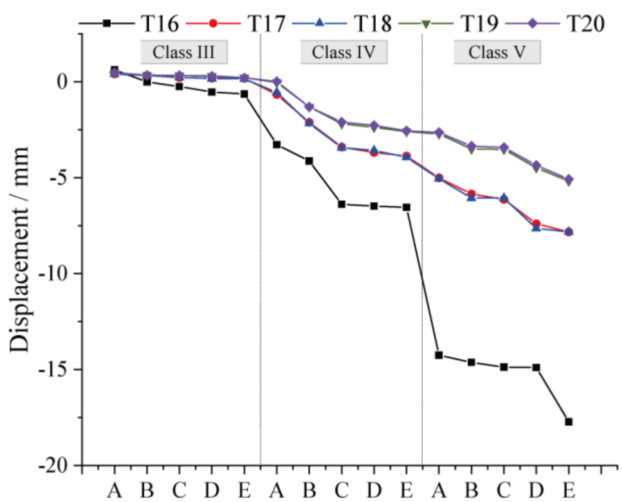

Figure 18: Displacement curves at monitoring points at the 2 d location

The numerical simulation results indicate that:

Among the monitoring points in each ring, the surrounding rock displacements follow a consistent order: crown > waist > invert. Under the same surrounding rock classification, the displacements at each monitoring point increase progressively with increasing excavation width; under the same excavation width, the displacements increase progressively with decreasing surrounding rock classification, meaning that deteriorating construction conditions lead to greater surrounding rock displacements.

Under identical excavation widths, the surrounding rock displacements in newly constructed three-lane or four-lane tunnels are lower than those in in-situ expanded tunnels. Therefore, in in-situ tunnel expansion projects, targeted support measures should be employed to enhance the tensile strength of the surrounding rock and prevent excessive displacements. Improving the self-stabilizing capacity of the surrounding rock is critical to the construction of expanded tunnels, particularly by reinforcing the rock mass above the crown to control the extension of tensile cracking zones and loose surrounding rock zones.

5.3. Surrounding Rock Loose Zone

In a non-uniform stress field, under specific conditions and within the elasto-plasticity theory, the plastic zone of the surrounding rock around a circular cavern exhibits three typical morphologies: circular, elliptical, and butterfly-shaped (Xiaofei G., 2019). Although these three basic morphologies of the plastic zone in circular caverns under non-uniform stress fields have been identified, they are primarily explicit manifestations based on idealized circular caverns, whereas most caverns in practical engineering are not perfectly circular.

In the numerical simulation of in-situ tunnel expansion, the existing tunnel has already formed an established loose zone in the surrounding rock during the in-situ stress equilibrium phase. During expansion construction, the plastically deformed surrounding rock is excavated, causing the loose zone to propagate outward, the surrounding rock stresses to redistribute, and shear or tensile failure to occur in the corresponding unloading zone.

In the State cloud map, markings are defined as follows: 0 for undamaged, 1 for current tensile failure, 2 for current shear failure, 4 for past tensile failure, and 8 for past shear failure. Given the 15 scenarios, only the State cloud maps of the surrounding rock loose zones for the "two-to-three" tunnel (i.e., expansion from two lanes to three lanes) under different surrounding rock grades are presented here. The simulated results for the tunnel surrounding rock loose zones under Class III to Class V conditions are shown in Figure 19.

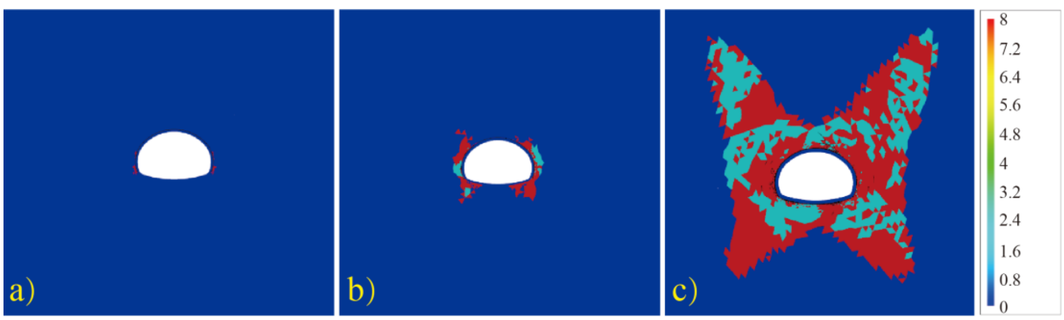

Figure 19: Tunnel surrounding rock loose zones under different surrounding rock classification: a) Class III; b) Class IV; c) Class V

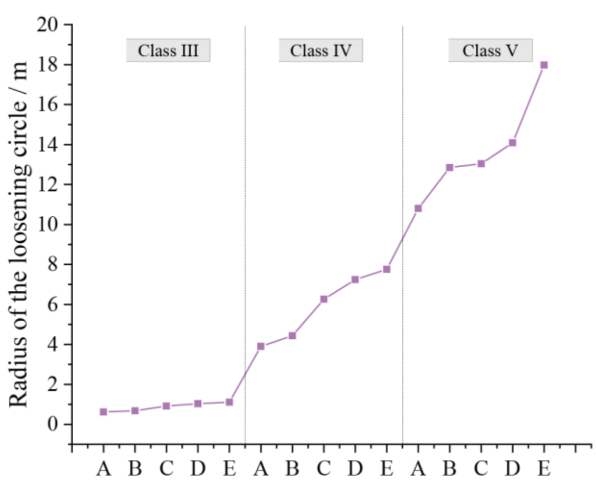

Figure 20: Maximum radius of the surrounding rock loose zone from different conditions

The numerical simulation results for the surrounding rock loose zones indicate that:

Under Class III surrounding rock conditions, regardless of whether it is a newly constructed or expanded tunnel, the loose zone appears only at the waist positions on both sides, with a very limited extent that can be regarded as point-like; as the tunnel span increases, the loose zone extent expands only slightly. Under Class IV conditions, the loose zone takes an ear-shaped form; as the tunnel span increases, the extent progressively expands, and the loose zone in expanded tunnels is larger than that in newly constructed tunnels. Under Class V conditions, the loose zone assumes a butterfly-shaped form; as the tunnel span increases, the extent progressively expands, and the loose zone in expanded tunnels is larger than that in newly constructed tunnels.

Under identical construction schemes, as the surrounding rock grade decreases, the tunnel loose zone extent progressively expands, with its morphology evolving from point-like to ear-shaped and further to butterfly-shaped. Under the same surrounding rock grade, the loose zone extent in newly constructed three-lane tunnels is smaller than that in "two-to-three" expanded tunnels; similarly, the extent in newly constructed four-lane tunnels is smaller than that in "two-to-four" expanded tunnels.

In summary, the disturbance and influence extent on the surrounding rock from newly constructed tunnels are less than those from expanded tunnels. The stress regime in expanded tunnels differs from the conventional conditions in newly constructed tunnels, as their initial stress and strain fields often result from multiple prior disturbances, with further perturbations occurring during the expansion construction process. This complex stress evolution leads to significant differences in the stress-strain fields between newly constructed and expanded tunnels, while also causing the originally stabilized surrounding rock loose zone to propagate outward once more.

6. Field Monitoring Data

To validate the accuracy of the numerical calculations and further quantify the impacts of in-situ tunnel expansion on the redistribution of surrounding rock stresses and the loading on support structures, field stress monitoring was conducted.

Based on the actual conditions of the expanded tunnel, monitoring cross-sections were arranged at 10 m intervals within the primary support range, with a total of three sections selected for monitoring: Section 1 at chain age ZK435+270, Section 2 at ZK435+280, and Section 3 at ZK435+290. Sections 1 and 2 are in Grade IV surrounding rock, while Section 3 is in Grade V surrounding rock. The monitoring instruments included anchor bolt dynamometers, strain gauges, and pressure cells, as illustrated in Figure 21.

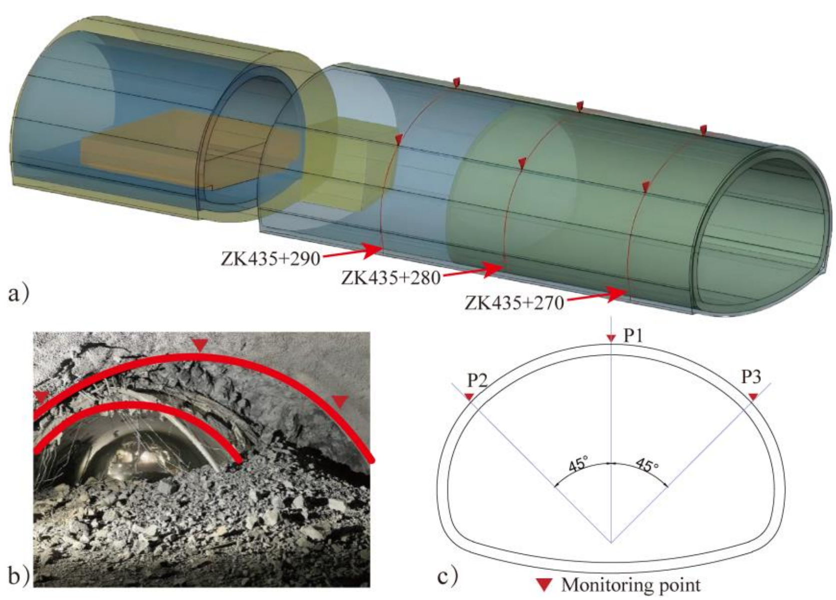

Figure 21: Field monitoring arrangement: a) Longitudinal layout of monitoring sections; b) Expansion excavation; c) Layout of monitoring point

Based on the construction workflow, the entire tunnel expansion excavation operation is divided into three main stages:

Stage I: Left-side construction. This stage employs a benching tunnelling method, encompassing the following four primary procedures in Table 8.

Table 8: Construction sequence of left-side construction using benching method

Sequence	Construction
1	Removal and excavation of the original lining for the upper bench on the left side of the existing tunnel.
2	Installation of primary support and temporary support for the left-side upper bench.
3	Removal and excavation of the original lining for the lower bench on the left side.
4	installation of primary support and temporary support for the left-side lower bench, to ensure progressive stability.

Stage II: Right-side construction. This stage focuses on the mirrored right-side operations, including right-side excavation and primary support installation.

Stage III: Expanded secondary lining construction. This stage achieves full-face closure, with primary procedures involving the pouring of the main tunnel invert and the secondary lining concrete.

6.1. Steel Arch Stress

The steel arch stresses measured during the in-situ expansion construction of the Tingxin Tunnel were plotted as stress-time relationship curves for three monitoring sections, as shown in Figure 22 to Figure24.

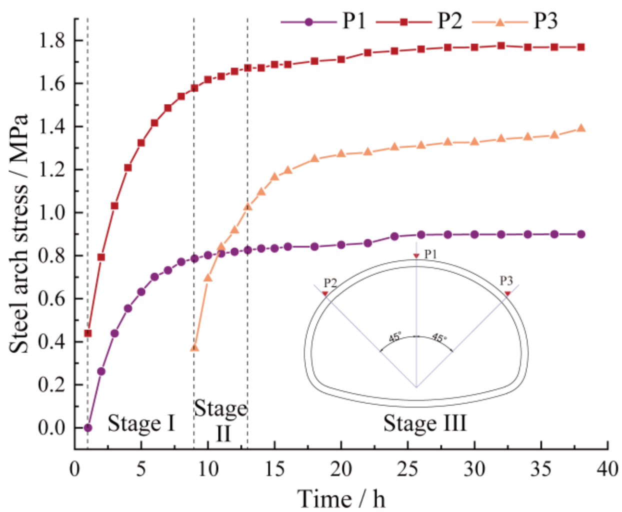

Figure 22: Time-varying stress curve of steel arch at section 1

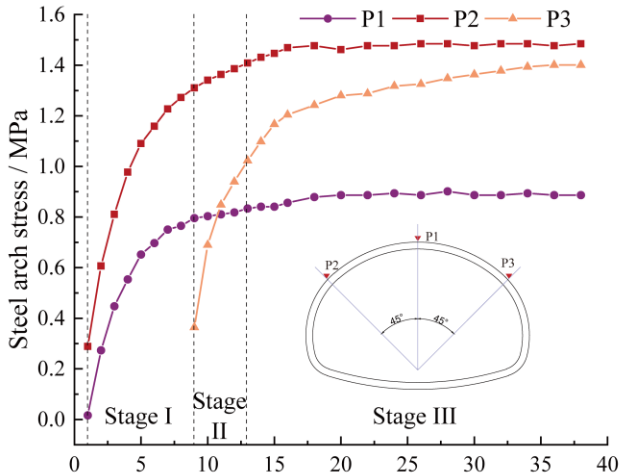

Figure 23: Time-varying stress curve of steel arch at section 2

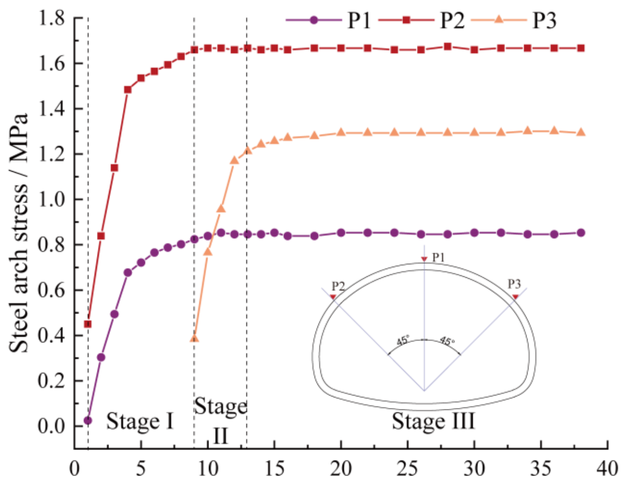

Figure 24: Time-varying stress curve of steel arch at section 3

The stress variation patterns of the steel arches are like those of the contact stresses between the primary support and the surrounding rock, primarily manifesting in three stages: rapid increase, gradual increase, and stabilization. Specifically, the steel arch stresses exhibited a rapid increase within the first 13 hours, followed by a deceleration in the growth rate; after the application of the expanded secondary lining, the stresses stabilized, and overall levels were slightly lower than the contact stresses between the primary support and the surrounding rock.

Upon stabilization of the steel arch stresses, the maximum stress occurred at the left waist position of section 1, reaching 1.77 MPa, while the minimum stress was at the crown of section 3, at 0.85 MPa.

6.2. Primary Support-surrounding Rock Contact Stress

The contact stresses between the primary support and the surrounding rock, measured during the in-situ expansion construction of the Tingxin Tunnel, were plotted as stress-time relationship curves for three chain ages, as shown in Figure 25 to Figure 27.

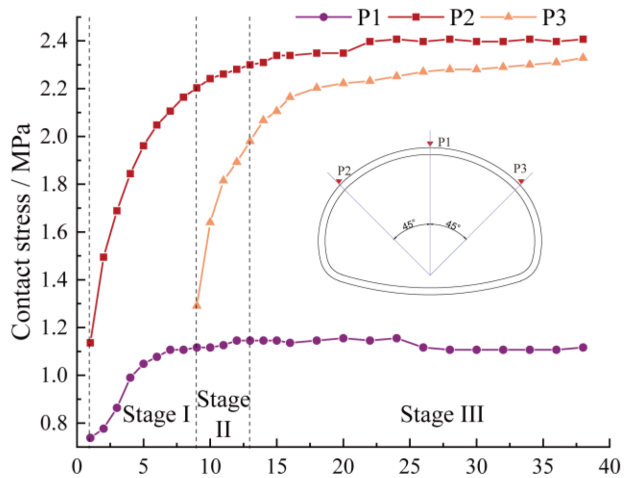

Figure 25: Time-varying curve of primary support-surrounding rock contact stress at section 1

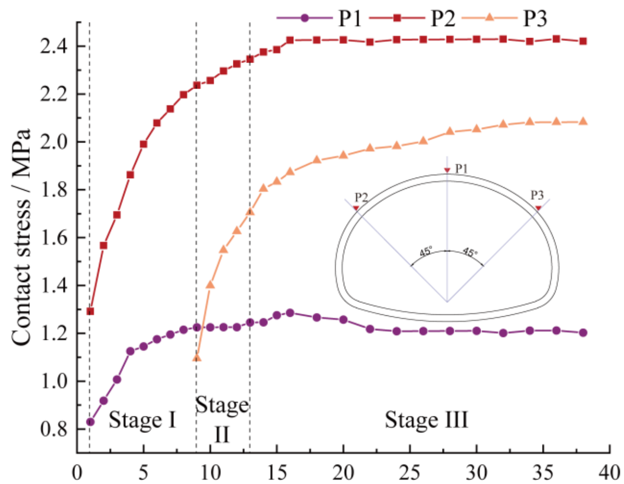

Figure 26: Time-varying curve of primary support-surrounding rock contact stress at section 2

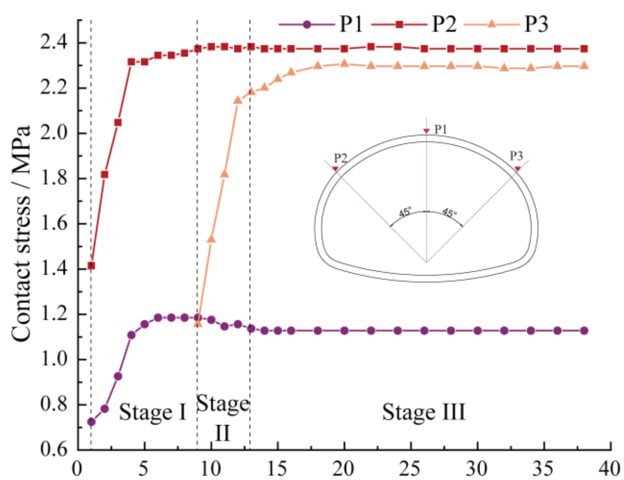

Figure 27: Time-varying curve of primary support-surrounding rock contact stress at section 3

The temporal variation patterns of the contact stresses between the primary support and the surrounding rock, as reflected in the three monitoring sections, are similar, primarily exhibiting three stages: an initial rapid increase stage, a subsequent gradual increase stage, and a final stabilization stage. Specifically, the contact stresses between the surrounding rock and the primary support varied significantly within the first 5 hours after installation, stabilizing around the 10th hour. Following the completion of the expanded secondary lining, the contact stresses increased gradually. The maximum value occurred at the left waist position section 2, reaching 2.42 MPa, while the minimum value was at the crown position of section 3, at 1.12 MPa.

Furthermore, the monitoring curves indicate that the contact stresses at the waist positions in all three sections were relatively high, and the excavation of the lower bench did not significantly alter the variation patterns of the contact stresses between the surrounding rock and the primary support. Thus, the excavation of the lower bench and the invert had minimal impact on the contact stresses at the waist, which gradually converged after the invert construction. It is recommended to enhance monitoring of waist stresses during the lower bench excavation process and to implement timely support measures post-excavation, particularly at the waist locations.

A comparative analysis of the contact stresses across the three monitoring sections reveals that the stresses at the waist measurement points were substantially higher than those at the crown points. The elevated stress values at the waist points can be attributed to their proximity to the upper and lower bench construction nodes; prior to the concrete solidification in the lower bench construction, these points were subjected to greater surrounding rock loads. Meanwhile, the lower bench construction had negligible influence on the contact stress variation patterns in previously completed sections.

An integrated analysis of the anchor bolt axial forces, steel arch stresses, and surrounding rock-primary support contact stresses from the three monitoring sections indicates that, during the in-situ tunnel expansion construction, these indicators exhibited significant variations prior to the application of the expanded secondary lining and stabilized thereafter. Their variation patterns were similar, primarily manifesting in three stages: a rapid change stage, a gradual change stage, and a stabilization stage. Prior to stabilization, the axial forces in the anchor bolts at the left and right waist positions increased progressively, whereas those at the crown position initially decreased slightly before rising gradually. This may be due to the gradual outward propagation of the surrounding rock loose zone during the in-situ excavation process, accompanied by an increase in the thickness of the pressure arch at the crown, leading to stress release in the surrounding rock. The subsidence of the pressure arch at the crown subsequently amplified the pressure on the waist positions, resulting in a minor initial reduction followed by a gradual increase in the crown anchor bolt axial forces, while the left and right waist anchor bolt axial forces rose progressively and then stabilized. The maximum contact stresses between the primary support and the surrounding rock, as well as the maximum steel arch stresses, were primarily concentrated at the left and right waist positions, with the minimum stresses at the crown, indicating that the excavation-induced stresses in the surrounding rock were predominantly released at the waist locations.

7. Conclusions

This study conducted numerical simulation analyses using the GDEM discrete element method for the in-situ expansion project of the Tingxin Tunnel on the Guangxi Hezhou to Bama Expressway (Du'an to Bama section), integrated with field monitoring data, yielding the following key conclusions and engineering recommendations:

1) The GDEM discrete element mechanics analysis software employed in this research effectively replicates the deformation processes, failure mechanisms, and outcomes of the surrounding rock, demonstrating high quantitative agreement with actual experiments and the reference engineering project, thus confirming the software's reliability and accuracy.

2) Following the completion of the in-situ tunnel expansion, the vertical stresses at various monitoring points in the tunnel primarily manifest as tensile stresses and exhibit a gradual decreasing trend over time. Therefore, implementing

targeted support measures to enhance the tensile strength of the surrounding rock during the expansion construction is crucial for preserving the rock's self-stabilizing capacity, with particular emphasis on reinforcing the tensile strength of the rock mass above the tunnel crown to prevent the formation of tensile cracking zones and loose rock areas, which should be prioritized in support design.

3) The thickness of the surrounding rock loose zone increased by 76.62% before and after the in-situ expansion construction, with the entire inter-tunnel rock wall entering the loose zone post-expansion, and the maximum extension occurring at the shoulder positions.

4) Pre-support or reinforcement of the surrounding rock prior to in-situ excavation in close-spaced tunnels can significantly improve the rock mass tensile strength and enhance the load-bearing capacity of the inter-tunnel rock wall. This approach holds substantial engineering significance for improving construction safety, mitigating collapse risks and associated economic losses, and accelerating overall project progress.

Acknowledgements

2020 Key Science and Technology Project of the Transportation Industry - Research on Key Technologies for Mechanized and Intelligent Expansion of Highway Tunnels (2020-ZD2-003); National Natural Science Foundation of China (52078089, 52274176); Yunnan Provincial Key Research and Development Program (202203AA080006); Science and Technology Demonstration Project for Safe and Intelligent Construction of Fengjian Expressway in the Three Gorges Reservoir Area [(2021)581]; Chongqing Talents Program for Leading Talents in Entrepreneurship and Innovation (CQYC20220302517); Chongqing Municipal Natural Science Foundation Innovation Development Joint Fund (CSTB2022NSCQ-LZX0079.

Author Contributions

W. S. finished the conceptualization, funding acquisition, methodology, software, investigation of the manuscript. **Z. L.** finished the writing, visualization, resources, editing and data curation of the manuscript. **H. Y.** finished the data curation, formal analysis and software. **S. D.** finished the data curation, writing of the manuscript. **H. W.** finished the supervision, conceptualization and resource of the manuscript. All authors critically reviewed and approved the final version of the manuscript and agreed to be accountable for all aspects of the work.

Disclosure of Interest

The authors declare that they have no known competing financial interests or personal relationships that could have appeared to influence the work reported in this paper.

Data Availability Statement

The data supporting the findings of this study are available from the corresponding author upon reasonable request.

References

Chen, L., Shi, P., Tang, Q., Liu, W., & Wu, Q. (2020). Development and application of a specification-compliant highway tunnel facility management system based on BIM. Tunnelling and Underground Space Technology, 97, 103262.

Dayong, H., Xingwu, Z., Lei, L., Hao, C., Dong, L., Zihai, Y., & Jiajia, Y. (2025). Study on the construction method for in-situ expansion of existing large cross-section tunnels. Discover Applied Sciences, 7(6), 556.

Feng, G., & Liu, F. (2017). Analysis on mechanical properties of surrounding rock of two-lane tunnel expanded into four-lane tunnel. Highway, 62(10), 288–293.

Xiaofei G. (2019). Criterion of plastic zone shapes of roadway surrounding rock and its application. [Master's thesis, China univeristy of mining&technology-Beijing].

Hu, J., & Huang, L. (2011). Study on deformation and mechanical properties of surrounding rock of in-situ expansion tunnel. Highway Traffic Technology, 2011(06), 83–87.

Huang, Z., Zhang, Y., Li, Y., Zhang, D., Yang, T., & Sui, Z. (2021). Determining tensile strength of rock by the direct tensile, Brazilian splitting, and three-point bending methods: A comparative study. Advances in Civil Engineering, 2021(1), 5519230.

Hernández, Y. Z., Farfán, A. D., & de Assis, A. P. (2019). Three-dimensional analysis of excavation face stability of shallow tunnels. Tunnelling and Underground Space Technology, 92, 103062.

Luo, Y., Chen, J., Shi, Z., Li, J., & Liu, W. (2020). Mechanical characteristics of primary support of large span loess highway tunnel: A case study in Shaanxi Province, Loess Plateau, NW China primary. Tunnelling and Underground Space Technology, 104, 103532.

Krupík, P. (2025). The Impact of Road Infrastructure Development on Selected Environmental, Economic, and Social Indicators. Civil and Environmental Engineering, 0(0), 2025. https://doi.org/10.2478/cee-2026-0022.

Li, L., Zhang, X., Deng, H., & Han, L. (2020). Mechanical properties and energy evolution of sandstone under uni-axial compression test at different loading rates. Journal of Mining and Strata Control Engineering, 2(04), 83–89.

Liu, K., Liu, Q., Zhu, Y., & Liu, B. (2013). Experimental study on Brazilian splitting and uni-axial compression of coal and rock considering bedding direction effect. Journal of Rock Mechanics and Engineering, 32(02), 308–316.

Meng, Q., Wang, H., Bai, L., Zhao, F. & Bai, J. (2025). Rock mass properties prediction method in TBM tunnel based on principal component analysis (PCA). Civil and Environmental Engineering, 0(0), 2025. https://doi.org/10.2478/cee-2026-0051.

Ministry of Transport of the People's Republic of China. (2018). Specifications for design of highway tunnels (JTG 3370.1–2018). China Communications Press.

Ministry of Transport of the People's Republic of China. (2025). 2024 Transport industry development statistical bulletin [Government report]. Ministry of Transport of the People's Republic of China.

Shu, Y., Jiang, S., & Lei, M. (2012). Construction mechanics analysis of expanded small clear distance highway tunnel. Journal of Chongqing Jiaotong University (Natural Science Edition), 31(02), 214–217, 251.

Wan, M., Hai, H., Liu, J., & Liu, B. (2006). Deformation stability monitoring and active control of surrounding rock in long-span tunnel excavation. Journal of Chongqing University (Natural Science Edition), 2006(07), 149–151.

Wu, Y., Liu, J., Wu, Z., Liu, J., Zhao, Y., Xu, H., & Zhong, W. (2024). A universal direct tensile testing method for measuring the tensile strength of rocks. International Journal of Mining Science and Technology, 34(10), 1443–1451.

Wu, Z., Xu, G., Wu, L., & Ye, Q. (2009). Study on mechanical characteristics of surrounding rock in lateral expansion construction of super large section tunnel. Journal of Geotechnical Engineering, 31(02), 172–177.

Yan, S., Wang, J. Q., & Xu, Y. D. (2024). The current status and prospects of integrated development of transportation and energy. Journal of Changsha University of Science and Technology (Natural Science Edition), 21(04), 1–27.

Yang, H., Gao, J., Ding, Y., Chen, X., Lin, Z., Wu, H., & Yang, Z. (2025). Mechanical response of broken surrounding rock by in-situ expansion of highway tunnel. Bulletin of Engineering Geology and the Environment, 84(5), 1–17.

Yang, S. Q., Ranjith, P. G., & Gui, Y. L. (2015). Experimental study of mechanical behavior and X-ray micro CT observations of sandstone under conventional triaxial compression. Geotechnical Testing Journal, 38(2), 179–197.

You, M., Chen, X., & Su, C. (2011). Brazilian splitting strength of dry and saturated rock discs and rings. Journal of Rock Mechanics and Engineering, 30(03), 464–472.

Zhang, J., Shi, B., Wang, J., Chen, Z., Gan, X., & Feng, J. (2021). Construction mechanics and safety analysis of "backfilling bench method" for in-situ expansion of four-lane highway tunnel in collapse section. Chinese Journal of Highway, 34(06), 109–124.

Zhang, S. (2019). Research on tunnel expansion technology [Master's thesis, Chongqing Jiaotong University].

Zheng, X., Huang, F., Wang, S., Zeng, Z., Chen, S., & Xu, W. (2025). Research on detection and treatment of loose zones in weak fracture zone tunnel. Scientific Reports, 15(1), 1075.

Zhong, Y. (2019). Field monitoring and analysis of in-situ expansion tunnel excavated by three-step construction method. Modern Tunnel Technology, 56(05), 170–179.

How to Cite This Article

Su, W., Lin, Z., Yang, H., Dang, S., & Wu, H. (2026). Mechanical Behaviour and Evolution of Rock Loosening Zone in in-situ Reconstruction and Expansion Construction of Highway Tunnels. Civil and Environmental Engineering, 0 (0). https://doi.org/10.2478/cee-2026-0077